

## Two-dimensional nanomaterials as emerging pseudocapacitive materials

Sul Ki Park, Puritut Nakhanej, and Ho Seok Park<sup>†</sup>

School of Chemical Engineering, Sungkyunkwan University (SKKU), Seoburo 2066, Jangan-gu, Suwon 16419, Korea  
(Received 11 June 2019 • accepted 15 August 2019)

**Abstract**—Supercapacitors have attracted significant attention as energy storage devices owing to their high power density, high charging rate, and long cycle life. However, they possess low energy density, which limits their practical applications. To address this issue, various high-capacitance materials, such as transition metal oxides and conducting polymers, have been investigated. Recent pioneering studies have described the emergent pseudocapacitance in two-dimensional (2D) nanomaterials, which are of significant interest because of their unique structure, remarkable physical properties, and tunable surface chemistry. Through this brief review, we present our contributions to this new class of pseudocapacitive 2D nanomaterials: oxidized black phosphorous, transition metal dichalcogenides, and MXene. The surface-capacitive charge storage mechanism of 2D nanomaterials is understood through in situ spectroscopic and computational analyses. Moreover, the corresponding capacitive features and performances are maximized by nanostructuring, nanoarchitecturing, and compositional control.

Keywords: 2D Nanomaterials, Charge Storage Mechanisms, Energy Storage, Pseudocapacitor

### INTRODUCTION

The depletion of fossil fuels and criticality of climate change have triggered an increasing demand for high-performance supercapacitors (SCs), which have important applications in rapidly growing markets such as power generation and electric vehicles (EVs) [1-3]. An SC (Fig. 1) is a type of secondary battery that was first proposed as an electric double-layer in 1853. A century later, it was eventually commercialized using high-surface-area activated carbon. As they possess high power density and semi-permanent cycle life, SCs are primarily used for memory back-up, in the production of hybrid EVs, and as a source of renewable energy and continuous power supply.

An electrochemical double-layer capacitor (EDLC) physically stores charge at the interface between an electrolyte and the electrode and is considered an attractive energy storage device owing to its higher power density and longer cycle life when compared to Li ion batteries. However, EDLCs exhibit low energy density (5-10 Wh/L), which limits their performance.

The energy density of a device is directly dependent on both the cell capacitance and cell potential, as shown in Eq. (1). SCs are classified as EDLCs, pseudocapacitors, and hybrid SCs, depending on the type of active materials used and the charge storage mechanism (Fig. 1). An EDLC stores energy by means of a non-Faradaic reaction, while the charge/discharge process occurs by means of a reversible surface Faradaic redox reaction in pseudocapacitors. Thus, pseudocapacitors offer higher energy density and capacitance when compared to EDLCs. Transition metal oxides, hydroxides, and conducting polymers are among the typical active materials used as pseudocapacitor electrodes. Hybrid SCs contain two electrodes based

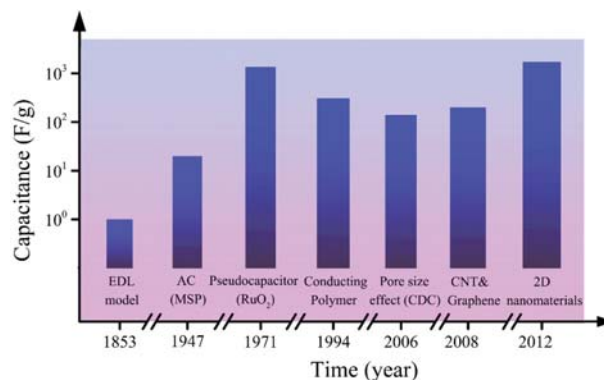


Fig. 1. History of SC: important materials and their storage capacitance [9].

on the storage mechanism of a battery and an SC, thus exhibiting power densities and energy densities between that of a battery and an EDLC.

$$E = \frac{1}{2} C_{cell} V^2 \quad (1)$$

E (Wh/kg): specific energy density;  $C_{cell}$  (F/g): specific capacitance of the SC cell; and V (V): cell potential

The specific capacitance of an SC ( $C_{sp}$ ) depends on the mass/volume of the electrode and quantity of electric charge, which is related to the energy density. As shown in Eq. (2),  $C_{sp}$  is determined from the area of electrode (A) and areal capacitance ( $C_{areal}$ ). For EDLCs, because  $0.2 e^-$  charge can be stored per atom of the active electrode material,  $C_{areal}$  is lower than  $30 \mu\text{C}/\text{cm}^2$ . For instance, even if single-layered graphene is ideally exfoliated from the bulk, the theoretical  $C_{sp}$  cannot exceed 550 F/g. To overcome this issue, research has focused on increasing the capacitance of pseudocapaci-

<sup>†</sup>To whom correspondence should be addressed.

E-mail: pbs0727@skku.edu

Copyright by The Korean Institute of Chemical Engineers.

tive materials ten-fold or hundred-fold.

$$C_{sp} = AC_{areal} \quad (2)$$

$C_{sp}$  (F/g): specific capacitance;  $A$  ( $m^2/g$ ): surface area of electrode;  $C_{areal}$  ( $F/m^2$ ): areal capacitance

Thus, pseudocapacitance can be increased via the electrochemical oxidation and reduction reactions on the surface of the electrode. Based on the operating mechanism involved, pseudocapacitors can be classified into three types [4].

First, in the case of underpotential deposition, pseudocapacitance occurs when metal ions are adsorbed as a single layer on the surface of another metal with higher reduction potential. Thus, although lead ions show pseudocapacitance on a gold electrode surface, there have been few reports of high-pseudocapacitive lead electrodes.

Second, intercalation pseudocapacitors exhibit pseudocapacitance upon the insertion of ions into the internal layers or tunnels in the active material, without any crystalline phase transition. The accelerated ion diffusion into the interlayers of  $Nb_2O_5$  was observed theoretically when dominated by the surface electrochemical behavior. However, it is difficult to discover new materials based on this mechanism.

Third, a redox pseudocapacitor displays pseudocapacitance when ions are electrochemically adsorbed onto the redox active sites on the surface of the electrode. Most pseudocapacitive materials such as hydroxides, conducting polymers, and doped carbon nanomaterials are redox pseudocapacitors and have been studied extensively.

Furthermore, transition metal oxides such as  $MnO_2$ ,  $NiO_2$ , and  $CuO$  have low electrical conductivity and long-term stability, while conductive polymers show relatively low chemical stability and cycle life.  $RuO_2$  exhibits capacitance only in an aqueous electrolyte with low potential and is expensive. Thus, there is an urgent need to develop high-capacitance pseudocapacitive materials for practical

applications.

Two-dimensional (2D) nanomaterials that are a few hundred nanometers in width can have molecular-level thickness and a large aspect ratio. In addition, they form strong covalent bonds in the in-plane direction and weak van der Waals forces between the respective surfaces. These results in special physical and chemical properties, as well as unique features such as large surface area to volume ratio, high redox activity on exposed surfaces, and unusual chemical reactivity, which are difficult to achieve in other dimensions or bulk materials. Particularly, because all the atoms on the surface of a single layer of 2D nanomaterials are exposed, various functionalities can be introduced by the physical and chemical control of the surface characteristics, which improves the properties of the materials. Professor Simon (identification of non-ideal capacitance increase by pore size control using carbide-derived carbon) [5], Professor Ruoff (first application of activated graphene as a SC) [6], and Professor Gogotsi (first application of 2D transition metal carbide as a SC) [7,8] were named Clarivate Citation Laureates for Physics, 2018, for their contribution to the field of carbon and 2D nanomaterials for capacitive charge storage. Thus, it is possible to develop a new pseudocapacitive material based on a 2D nanomaterial by the physical and chemical control of its surface structure. The focus is not necessarily on materials such as transition metal oxides and conductive polymers, which involve an intrinsic surface redox reaction. Herein, we briefly introduce pseudocapacitive materials developed by controlling the microstructure, surface chemistry, and morphology of a 2D nanomaterial [9].

## HYBRIDIZATION OF HIERARCHICAL STRUCTURED 2D TRANSITION METAL DICHALCOGENIDE

Various layered materials have been developed to replace com-

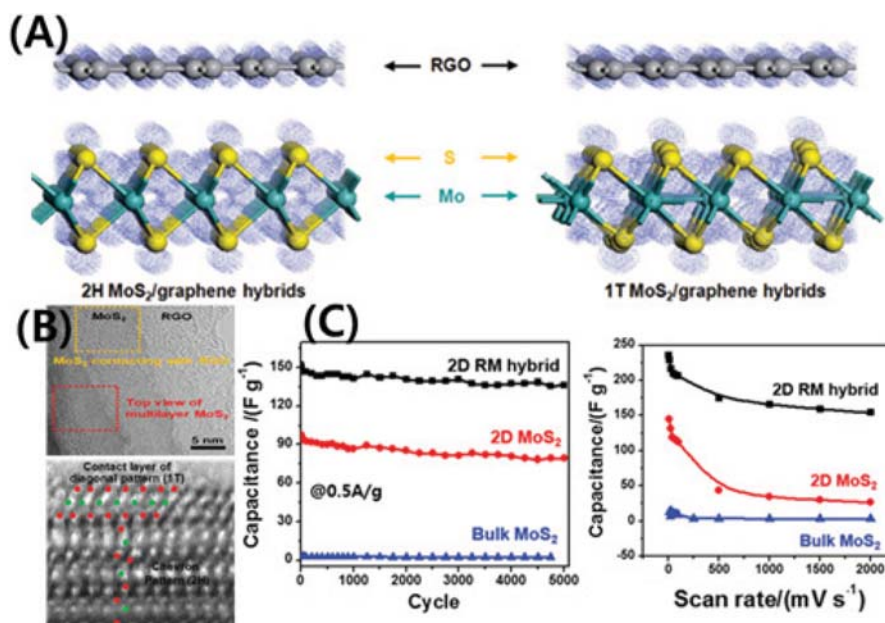


Fig. 2. (a) 3D schematics of the structural poly-types in the 2H MoS<sub>2</sub>/graphene hybrids and 1T MoS<sub>2</sub>/graphene hybrids. (b) TEM images of the 2D MoS<sub>2</sub>/graphene hybrids and HAADF-STEM images of MoS<sub>2</sub>. (c) Electrochemical characterization of 2D MoS<sub>2</sub>/graphene hybrids, 2D MoS<sub>2</sub>, and Bulk MoS<sub>2</sub> [20].

mercialized battery materials. However, solid-state diffusion limitations within interlayer spacing and slow charge transfer from the anisotropic structure result in low power density. A recent report detailed the difference between the charge storage mechanism of graphite as a commercial anode and that of exfoliated mono- or few-layered graphene. The electrochemical charge storage of graphite is derived from the intercalation mechanism implying battery-type behavior. In contrast, as the layered materials downscale into single-layer graphene, absorption and desorption are dominant on the exposed active sites at the surface, which implies double-layer capacitive behavior.

Many 2D transition metal oxides are used as electrodes for SCs because of their variable oxidation states and high surface area; these properties are different in their bulk forms [10-19]. We controlled the interface characteristics of layered molybdenum disulfide ( $\text{MoS}_2$ ) by hybridization with reduced graphene oxide (RGO) (Fig. 2). The transition of  $\text{MoS}_2$  from diffusive intercalation to surface redox charge storage behavior was observed when nanoscale sheets of layered  $\text{MoS}_2$  were heterostructured with RGO [20]. In addition, we determined the interface and chemical structures of the 2D  $\text{MoS}_2$ /graphene hybrids by density functional theory (DFT) calculations and various in-depth analyses; the charge transfer process appears to be facilitated by the strong interplay between 1T  $\text{MoS}_2$  and graphene. This is consistent with previous reports that the 1T phase of  $\text{MoS}_2$  exhibits high redox activity [17].

Additionally, we revealed the surface redox charge storage mechanism of a surface-exposed tungsten dichalcogenide ( $\text{WS}_2$ ) [21]. As shown in Fig. 3, we used RGO and  $\text{WS}_2$  nanosheets as the 2D building blocks for 3D macroscale architectures, which were synthesized through exfoliation of GO and  $\text{WS}_2$ , self-assembly combining colloidal and template chemistries, and reduction process. Unlike  $\text{MoS}_2$ ,  $\text{WS}_2$  film does not exhibit surface redox reactions

because of its long diffusion path in a tortuous structure. By contrast, 3D macroporous RGO/ $\text{WS}_2$  heteronanosheets show a fast and reversible pseudocapacitive behavior owing to facilitated ion diffusion through the 3D internetworked macropores and surface-exposed redox active sites in the 1T phase of  $\text{WS}_2$ . Besides, they achieve double capacitance of 299 F/g compared to a layered film structure, a high rate capability of 88.0%, and cycling stability of 98.8%. This indicates that assemblies of 2D nanosheets as the building blocks for 3D hierarchical architectures maximize the capacitive performance by promoting surface redox reactions.

The surface redox charge storage mechanism of the RGO/ $\text{WS}_2$  heteronanosheets was investigated using in situ Raman spectroscopy and synchrotron X-ray absorption spectroscopy (Fig. 4). During charge and discharge under operating potential ( $0.3\text{ V} \rightarrow -0.3\text{ V} \rightarrow 0.3\text{ V}$ ), there was a reversible structural change, confirmed by the change in composition and W-W interatomic distances ( $2.73\text{ \AA} \rightarrow 2.76\text{ \AA} \rightarrow 2.73\text{ \AA}$ ), from 2H to the 1T phase. The W-W distance increases after S atoms from  $\text{WS}_2$  interact with the fast protons entering the 3D structure, where the highly active 1T phase exists. To attain charge neutrality after the insertion of protons into the 3D matrix, the oxidation state of  $\text{W}^{4+}$  in the octahedral 1T phase becomes  $\text{W}^{(4-\delta)+}$ . During the desertion of protons, the reverse, including structural change and interactions, is observed. Thus, we have illustrated the novel surface-dominant charge storage mechanism of the 2D  $\text{WS}_2$  nanosheets, while also providing a fundamental understanding of the high electrochemical performance.

### CONTROL IN THE SURFACE STRUCTURE OF OXIDIZED BLACK PHOSPHOROUS NANOSHEETS

Black phosphorous (BP) is considered a promising battery electrode material owing to its high theoretical capacity of 2,600 mAh/

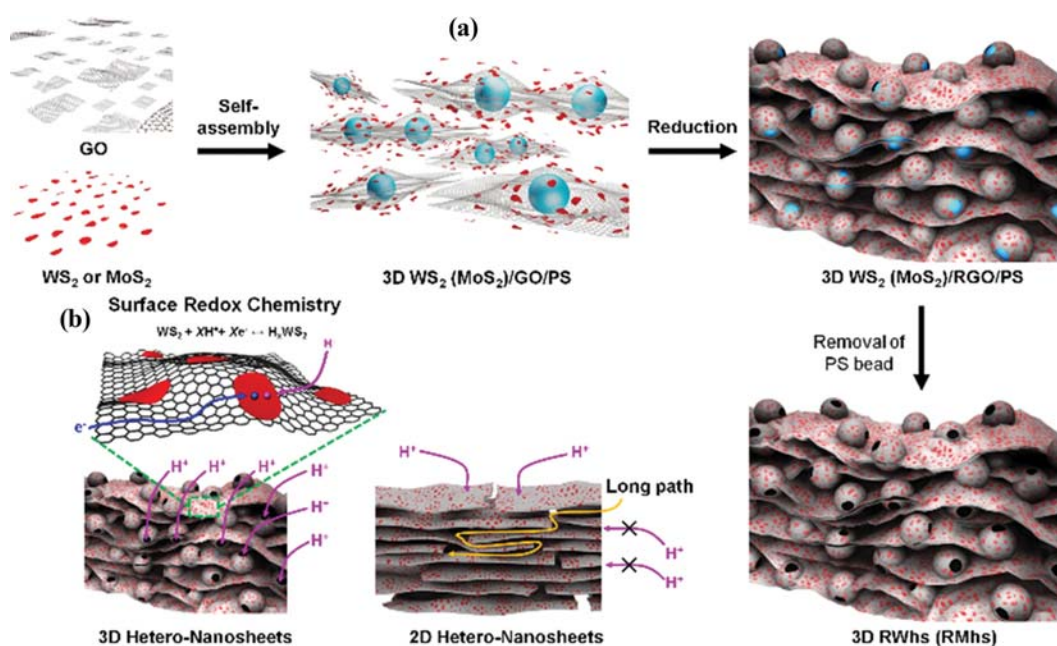


Fig. 3. (a) The synthesis of 2D  $\text{WS}_2$  and graphene nanosheets assembled 3D hierarchical architectures. (b) Comparison of ion diffusion in 3D hierarchical  $\text{WS}_2$ /graphene nanostructure and layered films with same composition [21].

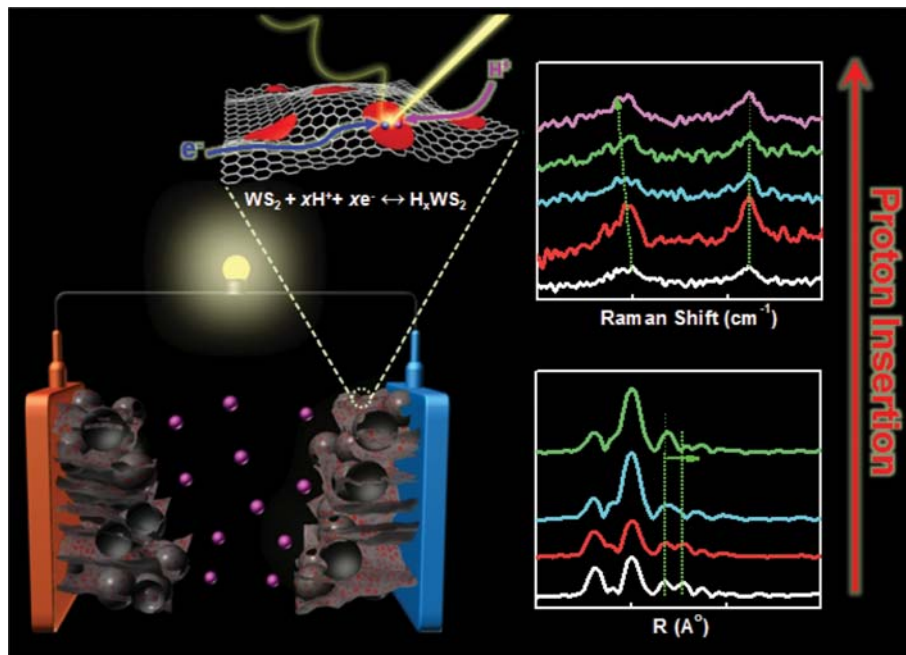


Fig. 4. Pseudocapacitor mechanism of 3D hierarchical structured WS<sub>2</sub>/graphene nanosheets using in situ Raman and X-ray absorption spectroscopy [21].

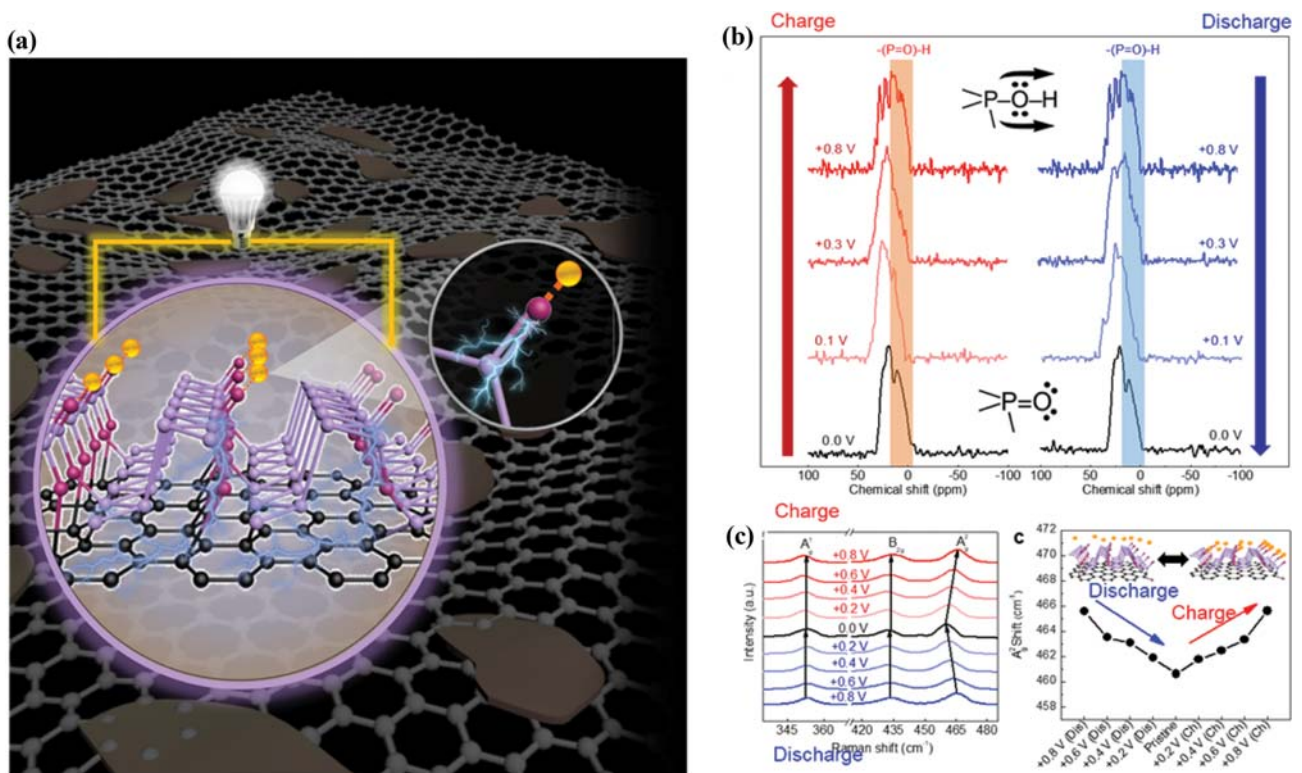


Fig. 5. (a) Schematic image of surface redox active P=O site of functionalized oBP/graphene. (b) In-situ <sup>31</sup>P NMR spectra of functionalized oBP/graphene as a function of applied voltage. (c) In-situ Raman spectra for the A<sub>1g</sub>, B<sub>2g</sub>, and A<sub>2g</sub> vibrations of the functionalized oBP/graphene at various charge-discharge potentials [25].

g, which is seven-times higher than that of commercial graphite. In addition, mono- or few-layered BP (similar to exfoliated graphene) shows unique physical properties. However, BP electrodes exhibit

low cyclic and rate capabilities because of their poor electrical conductivity and large volume change (>300%) upon Li storage.

Considering that the theoretical characteristics of energy stor-

age materials are limited by the intrinsic structure and/or charge storage mechanism, the structure of 2D BP has been currently investigated to improve the performance [22-24]. We demonstrated a new pseudocapacitive mechanism by controlling the molecular-level redox active sites to overcome the intrinsic limitation of BP [25]. In situ analysis and DFT calculations confirmed that a fast and reversible SC behavior is achieved by controlling BP. The surface redox pseudocapacitive features of surface modified BP resolve the limitation of sluggish kinetics and electrochemical instability previously reported for alloying/dealloying-based BP materials [25].

The molecular-level oxidation state obtained through ozone-driven chemistry resulted in an increase in the oxidation stability of BP. Subsequently, heat treatment was carried out to reduce the functional groups on GO, where the formation of covalent bonds resulted in strong interlayer coupling between redox-active oxidized BP (oBP) and electronically conductive RGO. This facilitated ultrafast charge transfer during the surface reaction through the conjugated structure of graphene via the shortened ion diffusion pathways from the graphene layer, while also chemically stabilizing the 2D oBP. In situ nuclear magnetic resonance (NMR) spectroscopy revealed that the P=O peak shifts reversibly during charge/discharge because the redox-active P=O sites bind with protons at the molecular level (Fig. 5).

In conclusion, we obtained a pseudocapacitance of  $478 \text{ F g}^{-1}$ , four-times higher than that of commercially available activated carbon (Fig. 6). The BP/graphene hybrid structure exhibited superior reversibility with coulombic efficiency of 99.6% at a high scan rate of  $50 \text{ A g}^{-1}$  and cycle stability of 90% after even 50,000 cycles. Our research also provides a fundamental understanding of the surface effects of 2D BP and a chemical approach for molecular-level control to

solve issues such as unstable cycle life and low rate capability of the existing alloying/dealloying of BP.

### POROUS ARCHITECTURE OF MXene/POLYMER HYBRID MATERIALS

Electrolytic capacitors have been applied as power devices for AC filtering in electronic circuits owing to their high-frequency operation. Supply of a constant voltage to an electronic device is possible by filtering the AC voltage generated by energy harvesting devices, as well as by eliminating voltage noise or ripple during electricity supply. However, the volumetric capacitance and device scalability have certain limitations. An energy storage device such as a battery has a high capacity; however, energy loss in the form of heat dissipation occurs at high frequencies. Thus, the application of energy storage devices is limited by the trade-off between the capacity and frequency response.

We demonstrated flexible electrochemical capacitors with a superior volumetric capacitance at high frequency using a porous MXene/conducting polymer hybrid and a gel-networked electrolyte [26]. The 2D MXenes are attractive pseudocapacitive materials for SC electrodes because of their good conductivity, high surface-to-volume ratio, and abundant active sites [7,27-33].

A large-area and flexible-film-type electrode of less than 100 nm was fabricated through a spray-coating process using  $\text{Ti}_3\text{C}_2$  MXene nanosheet and  $\text{Ti}_3\text{C}_2/\text{poly}(3,4\text{-ethylenedioxythiophene})$  polystyrene sulfonate (PEDOT:PSS) hybrid (Fig. 7); this provides high redox activity and faster ionic transport by controlling the nanoscale-porous structure. In addition, after double networking of polyvinyl alcohol and polyhydroxyethyl methacrylate, a gel electrolyte

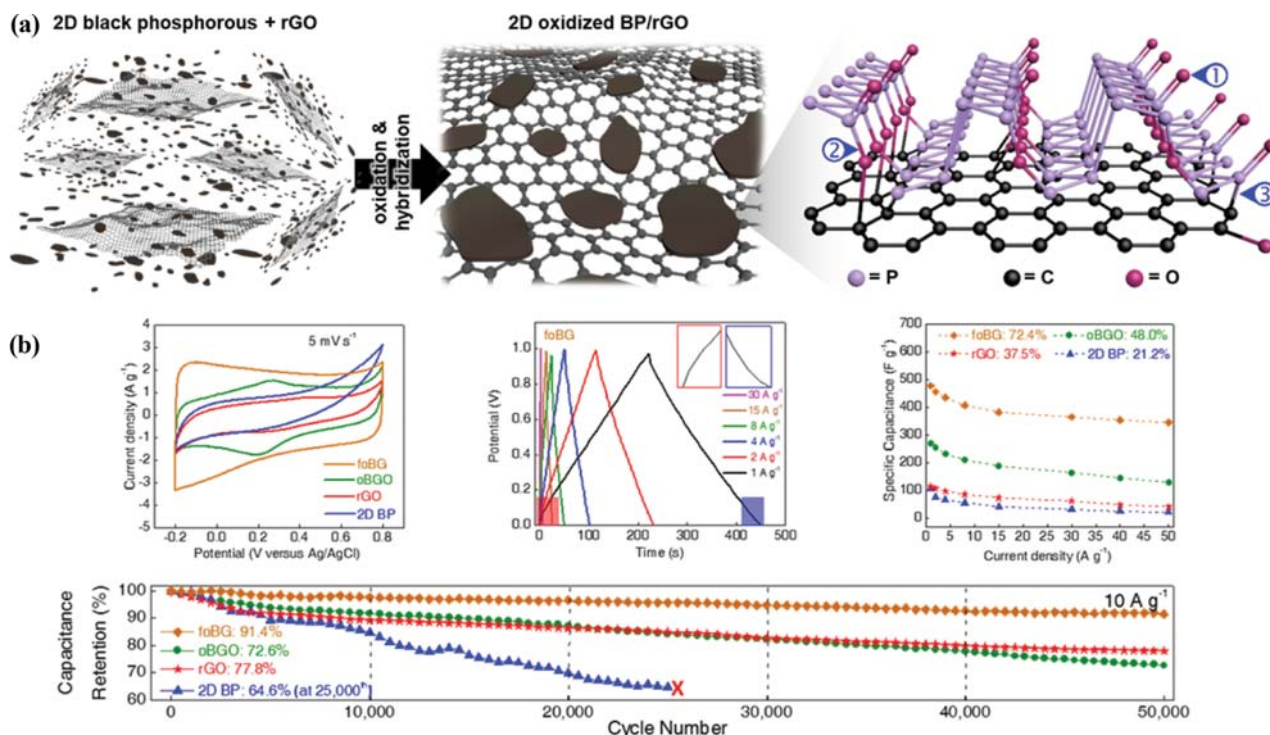


Fig. 6. (a) Synthesis and (b) electrochemical characterization of the functionalized oBP/graphene [25].

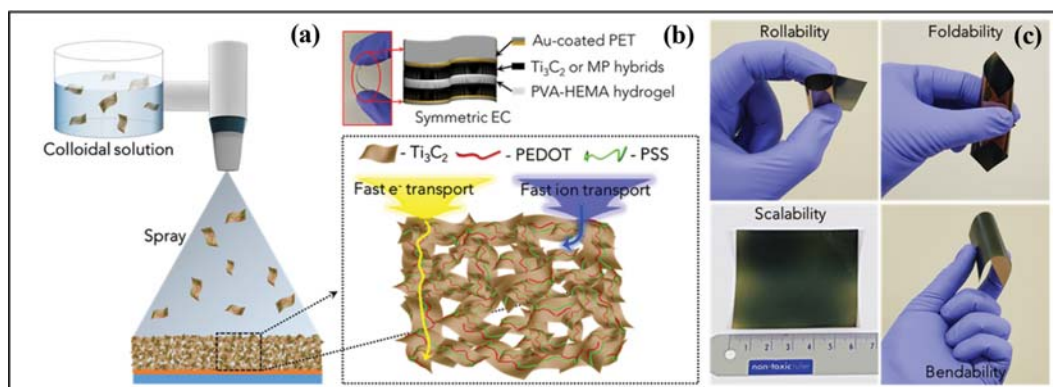


Fig. 7. (a) Schematic illustration of the fabrication of flexible  $\text{Ti}_3\text{C}_2/\text{PEDOT:PSS}$  hybrid electrode by the spray-coating method. (b) Cell configuration of symmetric ECs with two identical electrodes deposited on Au-patterned PET film and PVA-PHEMA networked hydrogel electrolyte. (c) Digital photographs show rolled, folded, bent, and flat states and scalability of hybrid electrode [26].

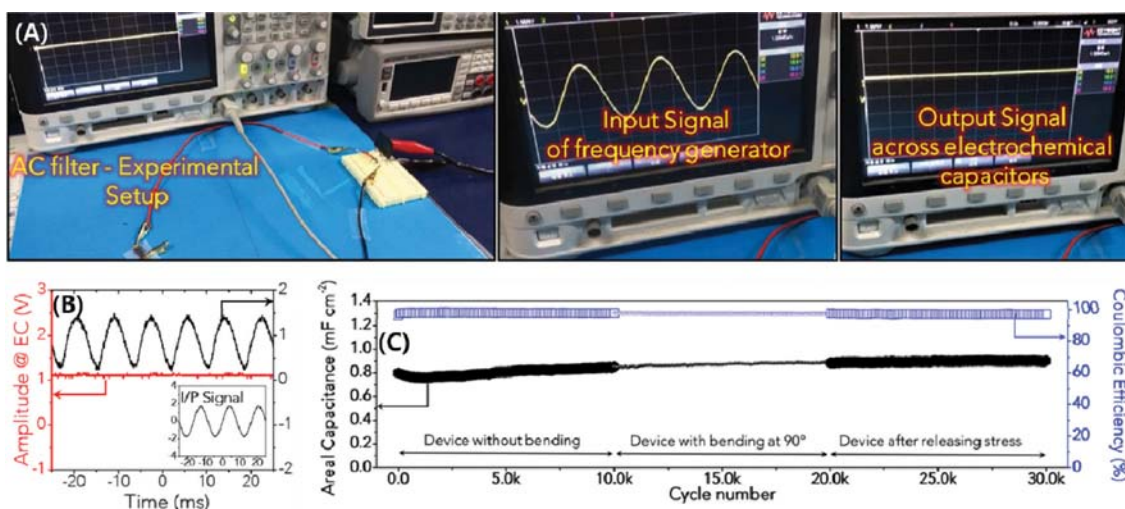


Fig. 8. (a) Panoramic digital photographs of real-life demonstration of AC filtering on cathode ray oscilloscope at 60 Hz. (b) Pulsating output signals across rectifier and constant DC output. (c) Capacitance retention and coulombic efficiency of MP 12 ECs over 30,000 cycles [26].

with excellent mechanical properties and high ionic conductivity was synthesized by absorption of 3M sulfuric acid in the networked structure.

The porous MXene/conducting polymer hybrid shows high capacitance at a rate of 1,000 V/s, from 60 to 10,000 Hz. Specifically, at 120 Hz, it shows high areal and volumetric capacitance of  $0.56 \text{ mF/cm}^2$  and  $24.2 \text{ F/cm}^3$ , respectively. Moreover, owing to its high volumetric capacity, it is possible to reduce the volume by more than 1,000 times when compared to a previously reported electrolytic capacitor. The mechanical deformation test, including bending and relaxing, shows their long-term durability over 30,000 cycles (Fig. 8). This study provides opportunities for designing various architectures with high area depending on the field of application.

## CONCLUSIONS

We have discussed surface redox pseudocapacitors obtained by physical and chemical control in the surface structure of 2D nano-

materials. The surface redox mechanism of 2D nanomaterials, such as  $\text{WS}_2$  and BP, was investigated by in situ spectroscopy and theoretical calculations. In the case of 2D MXene, a flexible AC-filtering SC was developed by overcoming the trade-off between capacity and frequency response. As shown in Fig. 9, the energy storage performance limitations of existing materials can be resolved by controlling the surface chemical composition, crystal structure, edges and defects, morphology, porous structure, and interface structure of 2D nanomaterials.

In the future, we will attempt to resolve various issues of 2D nanomaterials for practical energy storage applications, such as the types and optimized compositions of electrolyte and electrode, scalable synthesis of 2D nanomaterials, and fabrication of a thick and dense electrode. During materials synthesis and electrode fabrication processes, loss of intrinsic properties should be prevented. Suppression of the side reaction at the interface and interpretation of the energy storage mechanism by in situ spectro-electrochemistry and computer simulation need to be carried out as future directions.

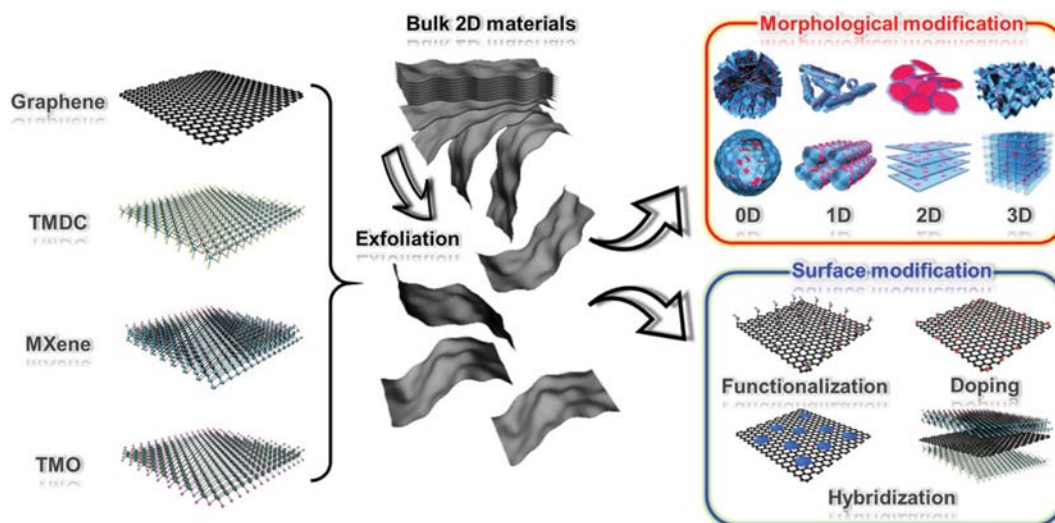


Fig. 9. Materials design for the new class of extrinsic pseudocapacitors based on 2D materials [9].

### ACKNOWLEDGEMENTS

This work was supported by both the Technology Innovation Program (20004958, Development of ultra-high performance supercapacitor and high power module) funded By the Ministry of Trade, Industry and Energy (MOTIE) and the R&D Convergence Program (CAP-15-02-KBSI) of the National Research Council of Science & Technology, Republic of Korea.

### REFERENCES

1. L. L. Zhang and X. Zhao, *Chem. Soc. Rev.*, **38**, 2520 (2009).
2. W. Raza, F. Ali, N. Raza, Y. Luo, E. E. Kwon, J. Yang, S. Kumar, A. Mehmood and K.-H. Kim, *Nano Energy*, **52**, 441 (2018).
3. D. P. Dubal, O. Ayyad, V. Ruiz and P. Gomez-Romero, *Chem. Soc. Rev.*, **44**, 1777 (2015).
4. V. Augustyn, P. Simon and B. Dunn, *Energy Environ. Sci.*, **7**, 1597 (2014).
5. J. Chmiola, G. Yushin, Y. Gogotsi, C. Portet, P. Simon and P.-L. Taberna, *Science*, **313**, 1760 (2006).
6. Y. Zhu, S. Murali, M. D. Stoller, K. Ganesh, W. Cai, P. J. Ferreira, A. Pirkle, R. M. Wallace, K. A. Cychoz and M. Thommes, *Science*, **332**, 1537 (2011).
7. M. R. Lukatskaya, O. Mashtalir, C. E. Ren, Y. Dall'Agnese, P. Rozier, P. L. Taberna, M. Naguib, P. Simon, M. W. Barsoum and Y. Gogotsi, *Science*, **341**, 1502 (2013).
8. M. Ghidui, M. R. Lukatskaya, M.-Q. Zhao, Y. Gogotsi and M. W. Barsoum, *Nature*, **516**, 78 (2014).
9. X. Yu, S. Yun, J. S. Yeon, P. Bhattacharya, L. Wang, S. W. Lee, X. Hu and H. S. Park, *Adv. Energy Mater.*, **8**, 1702930 (2018).
10. K. S. Kumar, N. Choudhary, Y. Jung and J. Thomas, *ACS Energy Lett.*, **3**, 482 (2018).
11. J. M. Soon and K. P. Loh, *Electrochem. Solid St. Lett.*, **10**, A250 (2007).
12. K.-J. Huang, L. Wang, J.-Z. Zhang, L.-L. Wang and Y.-P. Mo, *Energy*, **67**, 234 (2014).
13. G. Sun, X. Zhang, R. Lin, J. Yang, H. Zhang and P. Chen, *Angew. Chem. Int. Ed.*, **54**, 4651 (2015).
14. X. Yang, H. Niu, H. Jiang, Q. Wang and F. Qu, *J. Mater. Chem. A*, **4**, 11264 (2016).
15. L. Ren, G. Zhang, Z. Yan, L. Kang, H. Xu, F. Shi, Z. Lei and Z.-H. Liu, *ACS Appl. Mater. Interfaces*, **7**, 28294 (2015).
16. A. Khalil, Q. Liu, Q. He, T. Xiang, D. Liu, C. Wang, Q. Fang and L. Song, *RSC Adv.*, **6**, 48788 (2016).
17. M. Acerce, D. Voiry and M. Chhowalla, *Nat. Nanotechnol.*, **10**, 313 (2015).
18. G. A. Muller, J. B. Cook, H.-S. Kim, S. H. Tolbert and B. Dunn, *Nano Lett.*, **15**, 1911 (2015).
19. M. A. Bissett, S. D. Worrall, I. A. Kinloch and R. A. Dryfe, *Electrochim. Acta*, **201**, 30 (2016).
20. Q. Mahmood, S. K. Park, K. D. Kwon, S. J. Chang, J. Y. Hong, G. Shen, Y. M. Jung, T. J. Park, S. W. Khang and W. S. Kim, *Adv. Energy Mater.*, **6**, 1501115 (2016).
21. Q. Mahmood, M. G. Kim, S. Yun, S.-M. Bak, X.-Q. Yang, H. S. Shin, W. S. Kim, P. V. Braun and H. S. Park, *Nano Lett.*, **15**, 2269 (2015).
22. C. Hao, B. Yang, F. Wen, J. Xiang, L. Li, W. Wang, Z. Zeng, B. Xu, Z. Zhao and Z. Liu, *Adv. Mater.*, **28**, 3194 (2016).
23. X. Chen, G. Xu, X. Ren, Z. Li, X. Qi, K. Huang, H. Zhang, Z. Huang and J. Zhong, *J. Mater. Chem. A*, **5**, 6581 (2017).
24. H. Xiao, Z.-S. Wu, L. Chen, F. Zhou, S. Zheng, W. Ren, H.-M. Cheng and X. Bao, *ACS Nano*, **11**, 7284 (2017).
25. P. Nakhanejve, X. Yu, S. K. Park, S. Kim, J.-Y. Hong, H. J. Kim, W. Lee, J. Y. Hwang, J. E. Yang and C. Wolverton, *Nat. Mater.*, **18**, 156 (2019).
26. G. S. Gund, J. H. Park, R. Harpalsinh, M. Kota, J. H. Shin, T.-i. Kim, Y. Gogotsi and H. S. Park, *Joule*, **3**, 164 (2019).
27. S.-Y. Lin and X. Zhang, *J. Power Sources*, **294**, 354 (2015).
28. Y.-Y. Peng, B. Akuzum, N. Kurra, M.-Q. Zhao, M. Alhabeb, B. Anasori, E. C. Kumbur, H. N. Alshareef, M.-D. Ger and Y. Gogotsi, *Energy Environ. Sci.*, **9**, 2847 (2016).
29. M. Hu, Z. Li, G. Li, T. Hu, C. Zhang and X. Wang, *Adv. Mater. Technol.*, **2**, 1700143 (2017).

30. J. Zhu, Y. Tang, C. Yang, F. Wang and M. Cao, *J. Electrochem. Soc.*, **163**, A785 (2016).
31. J. Zhu, X. Lu and L. Wang, *RSC Adv.*, **6**, 98506 (2016).
32. Z. Ling, C. E. Ren, M.-Q. Zhao, J. Yang, J. M. Giammarco, J. Qiu, M. W. Barsoum and Y. Gogotsi, *Proc. Natl. Acad. Sci.*, **111**, 16676 (2014).
33. M. Q. Zhao, C. E. Ren, Z. Ling, M. R. Lukatskaya, C. Zhang, K. L. Van Aken, M. W. Barsoum and Y. Gogotsi, *Adv. Mater.*, **27**, 339 (2015).



Ho Seok Park is an associate professor of Chemical Engineering at SKKU as well as an adjunct professor at the Samsung Advanced Institute for Health Science & Technology (SAIHST). He received his Ph.D. from Korea Advanced Institute of Science & Technology (KAIST) in 2008 and worked as a Postdoctoral Researcher in the Department of Biological Engineering at Massachusetts Institute of Technology (MIT) from

2008 to 2010. His current research interests focus on energy and chemical storage materials and devices based on 2D, carbon, and hybrid nanomaterials. He has published more than 160 peer-reviewed papers on top journals, such as *Nat. Mater.*, *Joule*, *Energy & Environmental Science*, *JACS*, *ACS Nano*, *Nano Lett.*, *Adv. Mater.*, *Adv. Energy Mater.*, *Adv. Funct. Mater.*, and *Nano Energy*, and being taking editorial board member or associate editor in "Batteries & Supercaps" (Wiley), "Materials", "Carbon Letters", and "Macromolecular Research". He has been recognized with several awards including "100 Best Researches" (NRF, 2019), "The Scientist of the Month" (NRF, 2019), "Young Professor Award" (LG Chemicals, 2019), "SKKU Fellow" (Sungkyunkwan University, 2019), "SAIHST Arrow Award" (Samsung Advanced Institute of Health Science & Technologies, 2019), "Emerging Young Investigator" (RSC, 2018), "Best paper award" (KSIEC, 2016 & 2017), "Award for Young Researcher" (Miwon, 2017), "Top 3 Korean young researcher" (Jung Ang Ilbo, 2016), etc.